

# **JGR** Solid Earth

#### RESEARCH ARTICLE

10.1029/2025JB031813

#### **Key Points:**

- We present the first 3D resistivity model of Britain extending to a depth of 200 km based on long-period magnetotelluric data from 69 sites
- Model resistivity features match tectonic and geological structures, and reveal previously unidentified anomalies in the deep lithosphere
- Based on the model, we compute geoelectric fields for Britain during the October 2024 geomagnetic storm for space weather impact analysis

#### **Supporting Information:**

Supporting Information may be found in the online version of this article.

#### Correspondence to:

A. M. Montiel-Álvarez, a.montiel@ed.ac.uk

#### Citation:

Montiel-Álvarez, A. M., Hübert, J., Whaler, K., Beggan, C. D., Kiyan, D., & Hogg, C. (2025). The first three-dimensional electrical resistivity model of the lithosphere beneath Britain. *Journal of Geophysical Research: Solid Earth*, *130*, e2025JB031813. https://doi.org/10.1029/2025JB031813

Received 22 APR 2025 Accepted 14 SEP 2025

#### **Author Contributions:**

Conceptualization: Aideliz M. Montiel-Álvarez, Juliane Hübert, Kathy Whaler Formal analysis: Aideliz M. Montiel-Álvarez

Funding acquisition: Aideliz M. Montiel-Álvarez, Ciarán D. Beggan Methodology: Aideliz M. Montiel-Álvarez

**Project administration:** Ciarán D. Beggan

Resources: Duygu Kiyan, Colin Hogg Supervision: Juliane Hübert, Kathy Whaler, Ciarán D. Beggan Visualization: Aideliz M. Montiel-

© 2025. The Author(s).

This is an open access article under the terms of the Creative Commons

Attribution License, which permits use, distribution and reproduction in any medium, provided the original work is properly cited.

# The First Three-Dimensional Electrical Resistivity Model of the Lithosphere Beneath Britain

Aideliz M. Montiel-Álvarez<sup>1</sup>, Juliane Hübert<sup>2</sup>, Kathy Whaler<sup>1</sup>, Ciarán D. Beggan<sup>2</sup>, Duygu Kiyan<sup>3</sup>, and Colin Hogg<sup>3</sup>

<sup>1</sup>School of GeoSciences, University of Edinburgh, Edinburgh, UK, <sup>2</sup>British Geological Survey, Lyell Centre, Edinburgh, UK, <sup>3</sup>Geophysics Section, Dublin Institute for Advanced Studies, Dublin 2, Ireland

**Abstract** Magnetotelluric data provide unique information to study the electrical resistivity of the Earth's lithosphere, enabling studies of geological structures, tectonic processes, resource exploration, and hazard monitoring. Here, we present the first fully three-dimensional (3D) electrical resistivity model of the deep lithosphere beneath Britain (BERM-2024), derived from the inversion of long-period magnetotelluric data at 69 MT sites, incorporating recently acquired data along with selected legacy data sets. Rigorous testing of the prior model design and inversion smoothing parameters led to a robust and geologically meaningful model. The model reveals significant lateral and vertical variation, with shallow conductive anomalies correlating with sedimentary basins in western Britain, such as the Cheshire Basin and the Welsh Massif, while resistive anomalies are related to granitic plutons in the Scottish Highlands and Cornwall. At mid-crustal to upper mantle depths, strong resistivity contrasts coincide with major faults that bound distinct tectono-stratigraphic terranes, including a clear signature of the Southern Uplands Fault separating the conductive Southern Uplands Terrane from the less conductive Midland Valley Terrane. A newly imaged, deep conductive anomaly (~85-140 km) is detected beneath the West Midlands region. Beyond the geological insights, resistivity models are key for studying space weather impacts on ground-level infrastructure. We model geoelectric fields for the geomagnetic storm of 10 October 2024 using our model, demonstrating high correlation with measured electric fields at Eskdalemuir magnetic observatory (ESK), although amplitude discrepancies remain. This work establishes a foundation for future geophysical and geohazard studies and underscores the need for continued magnetotelluric data acquisition across Britain.

Plain Language Summary We used a geophysical method called magnetotellurics (MT) to investigate the underground structure of Britain. This technique measures how well rocks conduct electricity, parameterized by their electrical resistivity, which helps us learn about geological features beneath the surface. We created the first three-dimensional (3D) model of electrical resistivity beneath Britain, using data from 69 MT sites. The model shows clear differences across the country. Shallow high conductivity areas in western Britain are linked to sedimentary basins like the Cheshire Basin and Welsh Massif. In contrast, more resistive areas in the Scottish Highlands and Cornwall are likely related to granite bodies. At greater depths, the model highlights major geological boundaries such as the Southern Uplands Fault, where electrical properties change sharply between regions. A surprising finding is a large, deep conductive zone beneath the West Midlands region that has not been identified before. This model is also useful for understanding how solar storms might affect ground infrastructure like power grids. We tested our model during a strong storm in October 2024 and found a good match with measured electric fields, though some differences remain. Our work provides a foundation for future studies and highlights the need for continued MT surveys across Britain.

#### 1. Introduction

The electrical resistivity of the Earth's subsurface is highly variable at crustal and upper mantle depths. This physical property is very sensitive to partial melt and fluids in tectonically active crustal regions, whereas in tectonically stable regimes and in the mantle, the electrical resistivity is mainly controlled by temperature, hydrogen content, and graphite content (Selway, 2014). Imaging the distribution of the electrical resistivity, using electromagnetic deep-sounding methods such as magnetotellurics (MT), can therefore provide insights into the structure, composition, and geological evolution of the regional lithosphere.

The MT method uses simultaneous measurements of electric and magnetic field variations at the Earth's surface to probe the electrical resistivity of the subsurface using a broad range of frequencies in the natural electromagnetic

onlinelibrary.wiley.com/doi/10.1029/2025JB031813 by Anne Dixon

British Geological Survey, Wiley Online Library on [10/11/2025]. See the Terms and Condition

Writing – original draft: Aideliz M. Montiel-Álvarez Writing – review & editing: Juliane Hübert, Kathy Whaler, Ciarán D. Beggan, Duygu Kiyan, Colin Hogg

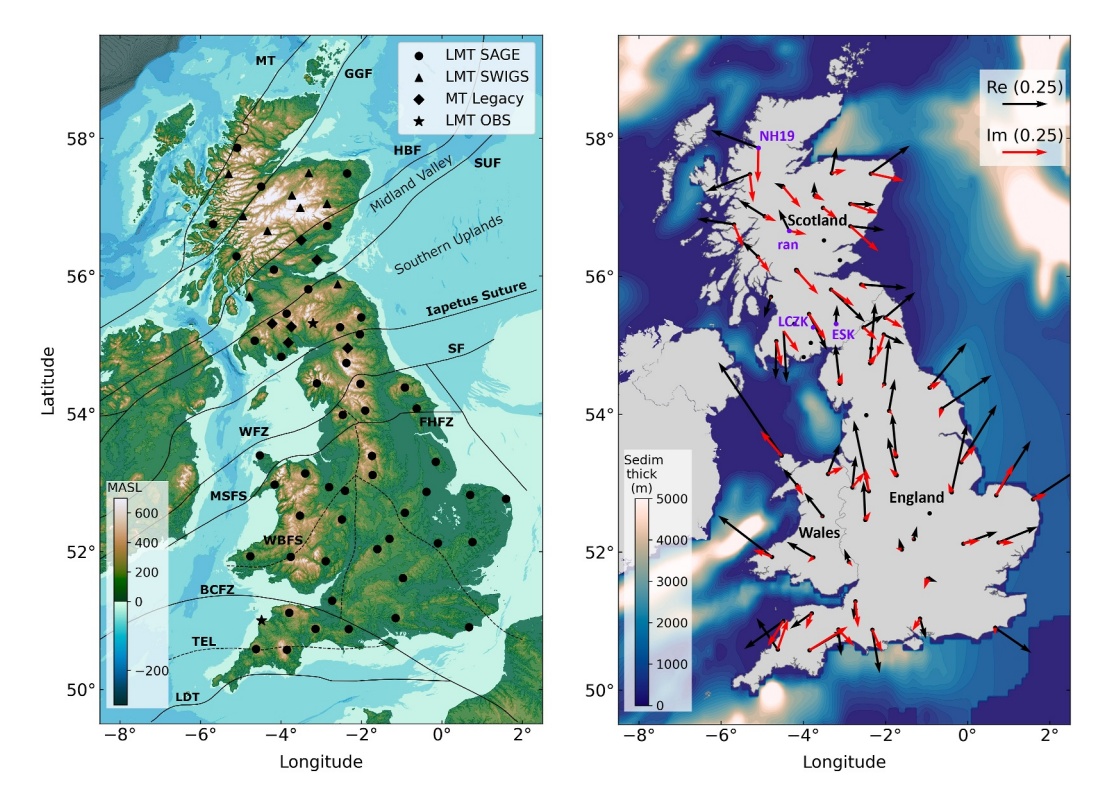


**Figure 1.** *Left*: Location of MT sites across Britain in bathymetry and elevation map (GEBCO Compilation Group, 2023). Geologic terranes and major fault systems are indicated by black lines, subterrane divisions indicated by dotted lines (adapted from Molyneux et al. (2023)). MT: Moine Thrust, GGF: Great Glen Fault, HBF: Highland Boundary Fault, SUF: Southern Upland Fault, IS: Iapetus Suture, SF: Stainmore Fault, WFZ: Wicklow Fault Zone, FHFZ: Flamborough Head Fault Zone, MSFS: Menai Strait Fault System, WBFS: Welsh Borderland Fault System, BCFZ: Bristol Channel Fault Zone, TEL: Tintagel-Exmouth line, LDT: Lizard-Dodman Thrust. *Right*: Model of marine sediment thickness around Britain from Grayver (2021) as used in the prior model, induction arrows at *T* = 2048 s (real arrows pointing toward conductors following Parkinson's convention), and names of selected sites discussed below (in purple).

spectrum. For periods larger than 10 s, it is referred to as long-period magnetotellurics (LMT) and penetrates to sufficient depths to resolve lithospheric-scale features. Given its ability to reveal electrical resistivity contrasts, the MT method has proven to be a useful tool in geothermal and mineral exploration, and monitoring of volcanic systems. Furthermore, research into continental structure and evolution, and the exploration of national mineral resources have motivated the emergence of large-scale and nationwide MT surveys such as the USArray (Schultz, 2009), SinoProbe (Dong et al., 2013), and AusLAMP (Stolz, 2013). Additionally, recent studies have shown that MT data are also useful to assess the impact of space weather in ground-level infrastructure (e.g., Campanyà et al., 2019; Hübert et al., 2024; Kelbert et al., 2017). With this motivation, LMT data were recently collected across Britain to establish the basis of a nationwide data set.

This paper presents the first 3D electrical resistivity model of Britain (BERM-2024) derived from the inversion of the new LMT data set and additional legacy data with the inversion code ModEM (Egbert & Kelbert, 2012; Kelbert et al., 2014). We describe the inversion workflow used to obtain the model, including data analysis and testing of model robustness and inversion parameters. We further present the island-wide estimates of geoelectric fields during the geomagnetic storm of October 10–11, 2024, using MT impedances from the resistivity model and magnetic fields measurements.

#### 1.1. Geological Setting of Britain

The British Isles have a complex tectonic history and a remarkably varied surface geology that comprises rocks from nearly every geological period. The foundations of Britain have been conceptualized in terms of tectonostratigraphic terranes (Bluck et al., 1992), each with a distinct internal geological history and bounded by prominent fault systems (Figure 1 left). The identification of a proto-Atlantic (Iapetus) ocean during the Lower

MONTIEL-ÁLVAREZ ET AL. 2 of 20

Paleozoic (Cocks & Fortey, 1982; Dewey, 1969; Wilson, 1966) revealed different origins for the terranes at each side: north of the Iapetus Ocean, the terranes that now form Scotland belonged to the paleo-continent Laurentia, while those now forming England and Wales were part of Gondwana. The closure of the Iapetus Ocean during the Caledonian orogeny (~480–380 Ma) is marked by the Iapetus Suture Zone (ISZ) with a prominent NE-SW orientation, which is found in much of the expressed surface geology and topology of northern parts of Britain and Ireland.

The Laurentian terranes are divided by steep faults that follow the same direction as the ISZ and are underlaid by a basement of Archean and Proterozoic metamorphic rocks. These are the oldest rocks in the British Isles and are widely exposed in the northernmost Hebridean Terrane forming the Lewisian Complex. The Northern and Central Highlands terranes are dominated by metasedimentary rocks of the Moine and Dalradian supergroups (Molyneux et al., 2023). The boundary between these two terranes, the Great Glen Fault (GGF), is a strike-slip fault originated toward the end of the Caledonian orogeny. There is strong consensus about early sinistral displacement, but less consensus exists on later phases of movement (Allen, 2019). The Midland Valley terrane is characterized by sediments and an ophiolite/arc igneous complex, and the Southern Uplands terrane, which is interpreted as an accretionary prism developed in a fore-arc region, comprises a series of fault-bounded sandstone and mudstone slices (Leggett et al., 1979).

In the Gondwanan margin, the Leinster–Lakesman and Monian Composite Terranes follow the same NE-SW strike as the ISZ and include rocks from volcanic arc environments, metamorphosed clastic and sedimentary sequences. Terranes to the south present more complex amalgamation as a result of the Varisican orogeny (~300 Ma) where the North Armorican terrane was accreted to the Cornubian and then this assemblage was transported laterally up against the Avalon Terrane. The Variscan event caused intense folding and deformation over south-west England, and a large granitic batholith was emplaced in Devon and Cornwall. The present-day surface geology is significantly influenced by Mesozoic extensional faulting, where the larger faults became major rift basins such as the Cheshire Basin, combined with posterior uplift and underplating in the Cenozoic (Holdsworth et al., 2012).

The crustal thickness in Britain has been estimated to be between 24 and 38 km, generally thickening from NW to SE, from different seismic studies (e.g., Davis et al., 2012; Licciardi et al., 2020), while the thermal lithospheric-asthenospheric boundary (LAB) has been estimated at ~100–150 km, thickening from west to east (e.g., Baykiev et al., 2018; Bott et al., 2024). For more information about the geological framework of Britain, readers are referred to the reviews of Holdsworth et al. (2012), Molyneux et al. (2023), and references therein.

#### 2. Previously Known Resistivity Structure and MT Data Sets in Britain

Deep-sounding electromagnetic studies have a long history in Britain. A large conductive anomaly was first identified from geomagnetic variations at Eskdalemuir and Glenlee in southern Scotland (Edwards et al., 1971; Osemeikhian & Everett, 1968), where the variations of the vertical magnetic field component at certain frequencies were noted to be much smaller than those at surrounding stations. Named the "Eskdalemuir anomaly" by Edwards et al. (1971), it was interpreted as a conductor in the lower crust. Bailey and Edwards (1976) then linked the conductive anomaly to potential oceanic crust remnants of the then-still-recently discovered Iapetus Ocean. This controversial idea motivated multiple geological and geophysical studies in southern Scotland and northern England to try to decipher the tectonic history.

The MT method was further developed and used by the electromagnetism groups at the University of Edinburgh and the British Geological Survey (BGS) from the end of the 1970s to mid-1990s. A series of long-period and broadband surveys was conducted across the Midland Valley, the Southern Uplands, and the Northumberland Basin in northern England (e.g., Banks et al., 1996; Harinarayana et al., 1993; Ingham & Hutton, 1982; Jones & Hutton, 1979a; Parr, 1991). The rapid development of MT instrumentation, codes, and computational capabilities, allowed the performance of 1D and 2D inversions of these data sets (e.g., Beamish, 1986; Ingham & Hutton, 1982; Jones & Hutton, 1979b; Livelybrooks et al., 1993; Parr, 1991). Their results improved the understanding of the complex electrical conductivity distribution in the area. A mid-crustal conductor was identified under the majority of the Southern Uplands and part of the Midland Valley. Banks et al. (1996) noticed that the conductor seemed to extend deeper into the Northumberland Trough, where a prominent resistive layer overlaid it. The broadband MT study from Tauber et al. (2003) in Galloway was the last one focused on the Iapetus Suture

In 2017, the UK Space Weather Impact on Grounded Systems (SWIGS) program, led by the BGS, restarted a new era of LMT acquisition in the UK. Nine sites collected in Scotland are used in this study. Two of them were recorded with a sampling rate of 1 Hz (Hübert & Beggan, 2022a, 2022b) and the rest at 32 s (Simpson & Bahr, 2020). As part of the subsequent Space Weather Innovation, Measurement, Modeling and Risk (SWIMMR) Activities in Ground Effects (SAGE) project (Huebert et al., 2022), 53 LMT sites were collected across Great Britain between 2021 and 2024 (Hübert, Eaton, Beggan, Collins, & Wang, 2025; Montiel-Álvarez et al., 2025). These data, recorded for 4–6 weeks at each site with a sampling rate of 1 Hz, are the basis for this study. Hübert, Eaton, Beggan, Montiel-Álvarez, et al. (2025) describe the data set and use it to develop a new ground electric field model for Britain. Finally, data from the Eskdalemuir (ESK) and Hartland (HAD) geomagnetic observatories, which continuously monitor both magnetic and electric fields at 1 Hz, were used as MT sites and as remote reference for processing the LMT data set. From all the available data, 69 MT sites were selected for this study (Figure 1).

#### 3. 3D MT Inversion Workflow

Inversion algorithms are essential to transform MT data into models of the subsurface electrical resistivity distribution. Despite the computational challenges posed by the non-linear and non-unique nature of the MT inverse problem, advancements in computational capabilities over the last two decades have made 3D MT inversion techniques both practical and tractable, establishing them as the standard for exploration surveys at any scale. However, the process remains bespoke as obtaining an adequate model and selecting inversion parameters are interrelated, specific to each data set, and vary depending on the inversion approach. Furthermore, the user introduces some degree of subjectivity when it comes to choosing those parameters (Miensopust, 2017). Detailed testing is therefore crucial to produce robust and geologically meaningful models.

In this study, we used the parallelized nonlinear conjugate gradient (NLCG) algorithm of ModEM (Kelbert et al., 2014). The inversion updates the resistivity model until it fits the MT data to within a specified misfit tolerance or a minimum misfit decrease. The process starts from a prior model built by the user, which includes dimensions and number of cells, and the initial resistivity value of those cells. Miensopust (2017) presented an extensive review of challenges and difficulties related to the preparation and performance of 3D inversions. Other studies (e.g., Lindsey & Newman, 2015; Robertson et al., 2020; Tietze & Ritter, 2013) have proposed guidelines to improve the inversion workflow, including error analysis, the choice of the initial resistivity model, prior information, and regularization parameters. Building upon these studies and our own experience, we present the inversion workflow developed to build the first 3D resistivity model of Britain.

#### 3.1. MT Data Preparation and Errors

Data preparation is a critical aspect of the inversion process. Firstly, the collected magnetic and electric field time series at each site are processed to derive transfer functions (TFs) at a discrete set of periods  $\omega$  (Kelbert et al., 2019). The TFs are the impedance tensor (Z), that relates the horizontal components of the electric (E) and magnetic (B) fields, and the vertical transfer function, so-called tipper (T), that relates the vertical to the horizontal components of the magnetic field. They are defined as:

$$\begin{bmatrix} E_x(\omega) \\ E_y(\omega) \end{bmatrix} = \begin{bmatrix} Z_{xx}(\omega) & Z_{xy}(\omega) \\ Z_{yx}(\omega) & Z_{yy}(\omega) \end{bmatrix} \begin{bmatrix} B_x(\omega) \\ B_y(\omega) \end{bmatrix}, \tag{1}$$

$$B_z(\omega) = \begin{bmatrix} T_{zx}(\omega) & T_{zy}(\omega) \end{bmatrix} \begin{bmatrix} B_x(\omega) \\ B_y(\omega) \end{bmatrix}. \tag{2}$$

The impedance tensor is often visualized as apparent resistivity  $(\rho_a)$  and phase  $(\phi)$  as a function of frequency, defined as:

MONTIEL-ÁLVAREZ ET AL. 4 of 20

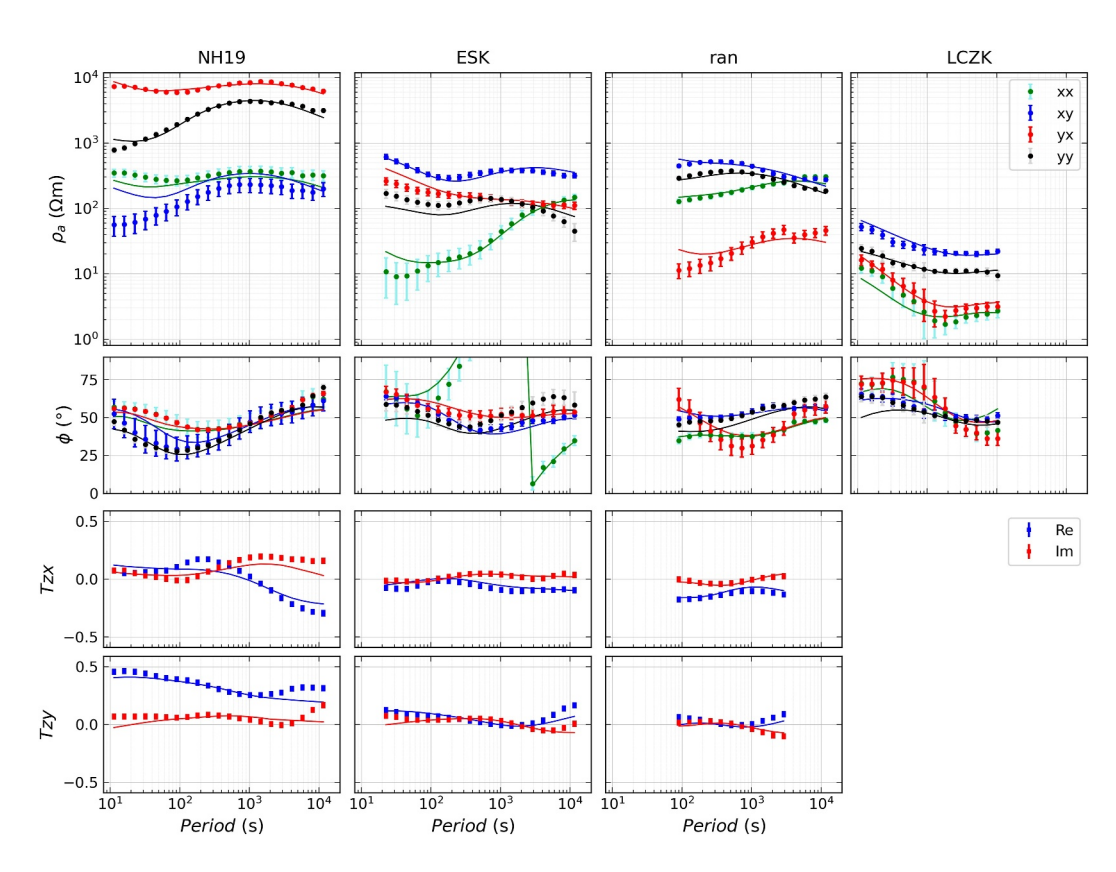


**Figure 2.** Apparent resistivity, phase, and tipper as a function of period at four MT sites from different data sets. Observed data shown as discrete points with error bars, and fit of the final model as continuous lines. Note that there are no tippers for the legacy data (such as LCZK). Location of these sites shown in Figure 1 (right).

$$\rho_{a_{ij}} = \frac{\left|Z_{ij}\right|^2}{\omega \mu_0},\tag{3}$$

$$\phi_{ij} = \arctan\left(\frac{\operatorname{Im}(Z_{ij})}{\operatorname{Re}(Z_{ij})}\right),$$
(4)

where i and j can be either x or y, and  $\mu_0$  is the magnetic permeability of free space.

We used the KMSProMT timeseries processing software to obtain impedance tensors and tippers for the SAGE and SWIGS data sets. KMSProMT uses the robust statistical procedure of Smirnov (2003) and incorporates remote referencing (Gamble et al., 1979; Goubau et al., 1978). In this method, remote magnetic field measurements with assumed uncorrelated noise are used as auxiliary fields to reduce bias in the local TFs. For this study, magnetic data from Eskdalemuir and Hartland geomagnetic observatories were used as remote reference. For the legacy data (Banks et al., 1996; Tauber et al., 2003), the original time series are not preserved and only the computed impedances were available.

During the 3D inversion process, the size of the data sets and specifically the number of frequencies used have an impact on the computational resources and inversion runtime; therefore, interpolation and smoothing were applied to standardize the impedance and tipper data at all sites to 21 frequencies within the range of 11–11,000 s. The SAGE data set and observatory sites have data in the full range (56 sites), while most of the SWIGS and legacy sites lack one decade of data due to differences in sampling rates and recording times. Figure 2 shows a selection of sites, each representing a different data set.

We use ModEM (Kelbert et al., 2014) for the 3D inversion to generate a plausible model from the impedance and tipper transfer functions. ModEM solves the MT inversion problem by minimizing a penalty function that

includes the multiplication of data vectors by the covariance matrix of the data errors. Thus, the error estimates are as important as the data themselves (Miensopust, 2017). The application of a minimum baseline error, called the error floor, is common practice to ensure stability of the inversion. Initially, we excluded a few sites due to poor data quality; for some others, only tippers were kept due to high noise levels in the recorded electric fields, which degraded the impedance tensor. During preliminary inversion tests, an initial selection of 11 legacy sites was reduced to six after finding that some of them not only had a poor fit but also negatively affected the fit of neighboring sites. A similar observation was reported by Moorkamp et al. (2022), who excluded problematic sites in their study. The tests here described were finally conducted with 64 sites, but 5 more sites in Scotland were added to obtain the final model because they were collected after the tests were done. Individual site inspection also led to the removal of noisy frequencies (highest or lowest) at a few sites. After several tests, we assigned an error floor of 5% of  $\sqrt{Zxy \cdot Zyx}$  to the impedance tensor. When the data uncertainties exceeded this floor, the actual errors were used. For the tippers, a constant error of 0.02 was assigned.

For the inversion process, the user defines a misfit threshold as one of the stopping criteria for the inversion. ModEM tries to minimize the overall normalized Root Mean Square (RMS) misfit between the model and the data. However, a single metric does not provide enough information about the inversion quality, and a closer analysis of the data misfit is necessary. Tietze and Ritter (2013) found that multiple models with similar "acceptable" misfits produced significantly different images of conductivity structures, concluding that the overall RMS misfit is not a reliable measure for evaluating inversion outcomes. They also pointed out the importance of systematic assessment of individual misfits and variations in the frequency-space domain. Here, besides the overall RMS misfit, we calculated the RMS misfit values of Z only, T only, and Z and T for each period decade to compare and select our preferred models. Similar to Robertson et al. (2020), we also quantified the variability among these misfits to find an equal weighting of the data components across the entire period range by computing the variance as:

$$Var_{RMS} = Var(RMS_Z, RMS_T, RMS_{10-100}, RMS_{100-1000}, RMS_{1000-10000}).$$
 (5)

#### 3.2. Model Discretization

When designing the model discretization, the spatial extent, depth, and grid cell size have a significant impact on data fit and computational time. The Finite Difference (FD) approach requires a regular discretization of the model space, usually in a Cartesian projection with a mesh of rectangular elements. A well-established practice is to design the mesh with a constant horizontal cell size in the survey area, adding padding cells that increase in size at a certain rate toward the model boundaries. The boundaries must be sufficiently far from the MT sites (or receivers) to comply with the boundary conditions and avoid adverse effects on the inversion results. Lindsey and Newman (2015) proposed placing the boundaries at 3–5 skin depths (the depth at which the electromagnetic energy is attenuated to a third of its surface amplitude) away from the closest receiver, based on the longest period of the data set. An alternative is to estimate the total horizontal dimensions based on the survey area. For example, Robertson et al. (2020) used a total horizontal dimension of about five and eight times the survey area in the north-south (NS) and east-west (EW) directions, respectively, while Hanneson and Unsworth (2023) used approximately seven times in both directions.

To investigate the cell size and dimensions of the model, we used a broadband MT survey from the Isle of Skye (Hautot et al., 2007) as a smaller pilot test before working on the whole of Britain. We tested dimensions 7, 5, and 3 times the survey area (denoted "7x," "5x," and "3x") (Montiel-Álvarez et al., 2022). We found that the overall RMS was very similar for the three model parametrizations with an expected decrease in computational time for smaller models. However, the 3x model was significantly different compared to the other two, including a more speckled appearance near the surface and strong deep anomalies around the study area. Based on these results, we concluded that five times the survey area is sufficient to avoid boundary effects while minimizing the number of padding cells. For the whole island of Britain, the survey area covers  $800 \times 500$  km in the NS and EW directions, resulting in total model dimensions of  $4260 \times 2432$  km. The total depth of the model was set to 2046 km, comparable to the minimum horizontal extent.

The cell size is a critical trade-off between resolution and computational resources. The mesh has to be fine enough to achieve accurate solutions at shallow depths (sampled by shorter periods) and approximate features like bathymetry, yet not so small that computational time and memory requirements become unrealistic (Jegen

et al., 2016). Miensopust (2017) noted that a cell size of about a fifth or a sixth of the site spacing is adequate in most cases. For instance, Meqbel et al. (2014) observed much better data fit when increasing the horizontal grid resolution from around one-third to one-sixth of the site spacing.

In cases of irregular site spacing, we recommend using the average or median distance. In our pilot study (Montiel-Álvarez et al., 2022), we tested cell sizes of 1/10, 1/6, 1/5, and 1/3 of the average site spacing. We found that a tenth was so small that it caused convergence problems. The final RMS values of the other three inversions were low and very similar; however, a loss in resolution was evident in the 1/3 cell size model. Therefore, we support the use of a fifth or sixth of the site (or average site) spacing. For this study, the spacing varies between 25 and 70 km, with an outlier of 130 km. The average and median distances are 44.7 and 44 km, respectively. We selected a cell size of 7.5 km (approximately one-sixth of the average/median site spacing) for all subsequent inversions. In the vertical direction, the first layer was set to 20 m thickness to better capture bathymetry and accommodate small-scale features, and the layer thickness increases with depth at a rate of 1.2.

#### 3.3. Resistivity of the Prior Model and Sequence of Data Components to Invert

ModEM penalizes deviations from a specified prior model (Equation 6), which is the reference model for the entire inversion process. This approach bears the risk that, while wisely chosen prior models can enhance the fitting, models that are very different from a realistic solution can steer the inversion in the wrong direction (Miensopust, 2017). Besides the initial resistivity, a priori information, such as coastlines and bathymetry, can also be included in the prior model. Electric currents in the conductive oceans, combined with the strong resistivity contrast at the land–sea boundary, can distort MT data—most notably in the tippers, but also in the impedance responses. This phenomenon, known as the coast effect (Parkinson, 1962), can affect inland LMT data recorded up to hundreds of kilometers from the coast. Moreover, Grayver (2021) showed that the coast distortion in EM responses is not only due to the high conductivity of the ocean but also of the seafloor sediments. For the British Isles, Ivannikova et al. (2018) found that the electric field is distorted practically everywhere by the coast effect.

Incorporating bathymetry and sediments into the prior model of the Isle of Skye helped to reduce the final RMS and the number of iterations required for the solution to converge. Consequently, we include a bathymetry model from GEBCO Compilation Group (2023) in all inversion tests and the final inversion, assigning an ocean resistivity of  $0.3~\Omega m$ . The effect of topography, studied through forward modeling, is negligible in Britain for the period range of our data set and is therefore not included. Sediment layers are also simulated by increasing the resistivity linearly from the seafloor to  $\sim 5~\text{km}$  depth maximum until matching the half-space resistivity (referred to as "gradient sediments" from now on). Ocean and sediment cells are fixed, meaning that the resistivity values of those cells are not modified throughout the inversion.

In addition to the prior model, a starting model can also be used in ModEM. The starting model contains the model perturbation from an inversion output and it can be used to re-start the inversion process without changing the reference (prior) model.

To determine the optimal resistivity for the prior model and the best strategy to invert impedances and tippers, we conducted a series of tests with three inversion strategies, described below. We also investigated the use of prior and starting models for strategies with three inversion steps.

- 1. Impedances only (Z); then using the output model as a prior or starting model to then invert both impedance and tippers  $(Z \rightarrow Z + T)$ .
- 2. Impedance and tippers simultaneously (Z + T).
- 3. Tippers only (T); then using the result as a prior or starting model and adding impedances  $(T \rightarrow T + Z)$ .

For Strategy 1, we tested three homogeneous half-space models with resistivities of 50, 100, and 300  $\Omega$ m, as well as two layered models: one based on 1D inversion of the determinant averaged apparent resistivity from all sites, and another one based on the global mantle conductivity model of Grayver et al. (2017). For Strategies 2 and 3, we tested only the models that performed best in Strategy 1.

To select the best output models, we consider (a) the overall normalized RMS, (b) the variance of RMS misfit,  $Var_{RMS}$  (Equation 5), and (c) the computational time (measured as 1000 Core-hours = 1 kCh). Table 1

Strategy	Component	Prior model	RMS overall	Var RMS	kCh	Output model ID
1	Z	50 Ωm	2.62	0.11	3.16	M1.1a
		$100~\Omega m$	2.72	0.12	3.13	M1.1b
		$300~\Omega m$	2.95	0.20	4.81	
		1D aver	2.76	0.13	3.82	
		1D global	5.15	1.25	6.10	
	$Z \rightarrow Z + T$	M1.1a	2.83	0.23	3.25	
		M1.1a (s)	2.92	0.25	2.18	M1.2a
		M1.1b	2.96	0.26	2.68	M1.2b
		M1.1b (s)	3.12	0.32	2.24	
2	Z + T	50 Ωm	3.04	0.17	2.77	
		$100~\Omega m$	2.82	0.16	4.78	M2.1b
		1D aver	3.13	0.17	3.77	
3	T	50 Ωm	1.87	0.42	2.62	M3.1a
		$100~\Omega m$	1.84	0.33	2.23	M3.1b
	$T \rightarrow T + Z$	M3.1a (s)	3.19	0.19	3.87	
		M3.1b	3.00	0.20	4.12	
		M3.1b (s)	2.93	0.19	3.83	

Note. Z: impedance, T: tipper. (s) indicates that the model was used as starting model instead of prior.

summarizes the results of these tests, and the complete set of metrics can be found in the Supporting Information S1. We find the best models were produced by:

- Strategy 1 with a homogeneous half-space of 50 Ωm to invert Z only, and using the output model as starting model to invert both Z and T. Although using a starting model gives a slightly higher RMS than a prior model, the computational time was reduced by a third.
- Strategy 2 with a homogeneous half-space of 100  $\Omega$ m.

#### 3.4. The Role of Marine Sediments in the Prior Model

The prior model tests showed that the overall RMS misfit is higher when inverting both impedances and tippers compared to inverting impedances only. This may result from the sensitivity of tippers to the coast effect. So far, the tested models accounted for bathymetry and gradient sediments, with both features fixed. However, Grayver (2021) states that knowledge of bathymetry, sediment thickness, and variability of electrical conductivity within these layers is required to accurately model the electromagnetic induction effect of ocean and marine sediments. Around the UK, the ocean depth is shallow, averaging around 100 m (Figure 1 left), while the marine sediments can exceed 5 km in thickness near the coasts (Figure 1 right). This emphasizes the importance of closely examining the effect of marine sediments in the prior model.

We incorporated the global sediment thickness and conductance models from Grayver (2021) (Figure 1, right) to assign variable marine sediment conductivity in our models (hereafter referred to as "global sediments"). Additionally, we tested the hypothesis that freeing the sediment cells (i.e., allowing their conductivity to vary) when adding tippers would improve the data fit. Table 2 summarizes the results of these tests.

The first observation is that the RMS misfit is lower when using fixed global sediments compared to fixed gradient sediments, with only a slight increase in computational time. Second, freeing the sediment cells in both cases significantly reduced the RMS misfit, confirming our hypothesis. Interestingly, and contrary to the expectations that freeing additional cells would require more computational time, inverting the model with free global sediments took nearly the same time as those with fixed sediments. This suggests that incorporating more accurate marine sediment information not only improves the data fit but also accelerates the convergence.

Wiley Online Library on [10/11/2025]

Strategy	Component	Prior model	Sediments	RMS overall	Var RMS	kCh	Output model ID
1	$Z \rightarrow Z + T$	M1.1a (s)	Global fixed	2.65	2.07	2.23	
			Gradient free	2.24	1.79	2.47	
			Global free	2.28	1.77	2.26	M1.2a.3c
2	Z + T	$100~\Omega m$	Global free	2.34	1.79	4.69	
Strategy	Component	Prior model	Lambda	RMS overall	Var RMS	kCh	Output model ID
1	$Z \rightarrow Z + T$	M1.2a.3c	10	2.27	1.76	0.51	_
		M1.2a.3c (s)	10	2.11	1.63	2.67	
			100	7.86	5.97	2.25	

#### 3.5. Test of Smoothing Parameters

ModEM aims to minimize a penalty function that considers the difference between observed and calculated data, and smoothed deviations from a prior model:

$$\Phi(m,d) = (d - f(m))^T C_d^{-1} (d - f(m)) + \lambda (m - m_{prior})^T C_m^{-1} (m - m_{prior}).$$
(6)

where d is the observed data, m the conductivity model, f(m) the forward response of m,  $C_d$  the data covariance,  $m_{prior}$  the prior model.  $\lambda$ , the regularization parameter, is a smoothing parameter that, in conjunction with  $C_m$ , the model covariance, offers a trade-off between data misfit and model structure.

The covariance parameter is strongly related to the cell size and is assigned values between 0 and 1, where larger values produce smoother models, that is, suppressing strong resistivity contrasts between neighboring cells. Based on previous experience, we only tested covariance values of 0.2, 0.3 and 0.4, applying the smoothing twice in the three model directions. The initial value of the regularization parameter is assigned by the user at the start of the inversion, but then subsequently decreases throughout the inversion to allow the model to progressively better fit the data by introducing smaller-scale features and higher resistivity contrasts (Robertson et al., 2020). The initial  $\lambda$  commonly takes values in powers of 10. Both parameters impact on the resulting data fit and computational time, so it is important to test different values. The tests of initial resistivity and data components to invert were conducted with a covariance of 0.2 and  $\lambda = 1$ . In order to evaluate the behavior of these parameters, we tested different values for different strategies and prior models. All test results are listed in the Supporting Information S1.

We found that the inversion with a covariance value of 0.4 failed to converge, while the other values did not improve on the results obtained with 0.2, either visually or in terms of misfit. Therefore, we selected a covariance of 0.2 for the final inversion. The tests of the regularization parameter showed that the default value of  $\lambda=1$  was optimal for both steps of Strategy 1. However, restarting the inversion using the best output model with  $\lambda=10$  helped to further reduce the RMS misfit.

### 3.6. Inversion Workflow Summary

After these tests, the parameters and inversion steps chosen to obtain the final model are as follows:

- The model grid has a horizontal cell size of 7.5 km in the survey area, and padding cells that increase at a rate of 1.2 to the boundaries of the model. The total dimensions are approximately five times the survey area, resulting in model dimensions of  $2432 \times 4260 \times 2200$  km in the x, y, and z directions, respectively.
- The prior model includes bathymetry with an ocean resistivity of 0.3  $\Omega$ m, global marine sediments with variable resistivity and thickness, and a 50  $\Omega$ m homogeneous half-space.
- The inversion steps followed were: (a) Invert impedances (Z) with a homogeneous prior model of 50 Ωm and fixed ocean and global sediments. (b) Use the output model as a starting model to invert both impedances and tippers (Z → Z + T) with free sediment cells. Both steps used a covariance of 0.2 and initial λ = 1. (c) Restart the inversion using the output of the previous step as a starting model and with λ = 10.

While these parameter values are specific to our data set, the following steps and recommendations based on our experience can be applied to the 3D inversion of other MT data sets, particularly to relatively sparse LMT regional surveys and island settings:

- 1. A horizontal cell size of a sixth of the average or median site spacing is a good balance between resolution and computational time. If uncertain, test sizes between a fifth and a seventh.
- 2. Total model dimensions of five times the survey area seems to be enough to avoid boundary effects and minimize the number of padding cells.
- 3. Covariance values for the chosen cell size of between 0.2 and 0.4 produce the best results. The optimal remains consistent throughout subsequent inversion steps, so the covariance does not need to be changed after initial tests.
- 4. Including bathymetry and marine sediments in the prior model is necessary for surveys near and surrounded by seawater. If uncertain, test their influence. Accurate sediment information improves both RMS misfit and computational time.
- 5. Test the resistivity of the prior model. The components to invert can be tested simultaneously (e.g., Z + T, Z → Z + T). In multiple inversion steps, using the previous model output as starting model rather than prior model reduces computational time with similar or improved RMS misfit.
- Restarting the inversion from the last output with a higher λ can help to move out of a local minimum and decrease the RMS misfit.

#### 4. The 3D Resistivity Model of Britain

The preferred resistivity model (BERM-2024) was obtained through the 3D inversion of 69 LMT sites with the strategy described in the previous section. The overall RMS misfit was 1.84, with a lower misfit for impedances (1.69) than tippers (2.13). Within the modeled period ranges, the best data fit was achieved for 100–1000 s, while the largest RMS misfit occurred for the range of 10–100 s. Figure 4 (left panel) shows the RMS misfit at each site, where it can be seen that some of the higher misfits are in sites along the west coast. This may be due to the difficulty in modeling the rugged coastline using relatively large square cells (7.5 km), as well as the strong resistivity contrast between the conductive ocean and sediments and the resistive metamorphic rocks, particularly in Anglesey and northwest Scotland. Data fit at some sites can be seen in Figures 2 and 5.

The model is presented as horizontal slices at a series of crustal and upper mantle depths in Figure 3 and cross-sections in Figure 9. For depths down to 45 km the model displays a complex resistivity distribution that reflects the geology of Britain. Between 45 and 80 km depth the model shows less lateral resistivity variation with average values of around 150  $\Omega$ m and including only a few conductive features that remain as roots of shallower strong conductors. Further down, a strong conductor (<10  $\Omega$ m), aligned NW-SE in the West Midlands region, is present between depths of 85 and 200 km with a surrounding average resistivity of ~200  $\Omega$ m. In what follows, we conduct sensitivity and model robustness tests to determine the depth of investigation and, especially, if the deep conductor is well constrained. Finally, we describe major anomalies in the context of known geologic and tectonic structures in Britain.

#### 4.1. Sensitivity Tests

The maximum depth of model resolution depends non-linearly on the frequency range of the data and the electrical resistivity distribution itself. Longer periods and a resistive subsurface allow resolution at greater depths, while the presence of conductors can severely limit the penetration depth. To investigate this dependency in BERM-2024, we conducted a simple robustness test by modifying the resistivity of the model at selected depths, and computing the forward response of these modified models, to then calculate a relative misfit change for each site from Equation 7 that would describe the sensitivity of the data to the model perturbation.

% relative misfit change = 
$$\frac{\text{site\_RMS}_{modified} - \text{site\_RMS}_{final\_model}}{\text{site\_RMS}_{final\_model}} \times 100\%$$
 (7)

We changed the model resistivity to be a constant value of  $200~\Omega m$  below three different depths: 400, 280 and 200~km. Figure 4 shows the RMS misfit of each site for the final model and the relative RMS misfit change for two of the test cases. When the model has uniform resistivity below 200~km, 82% of the sites show relative RMS misfit

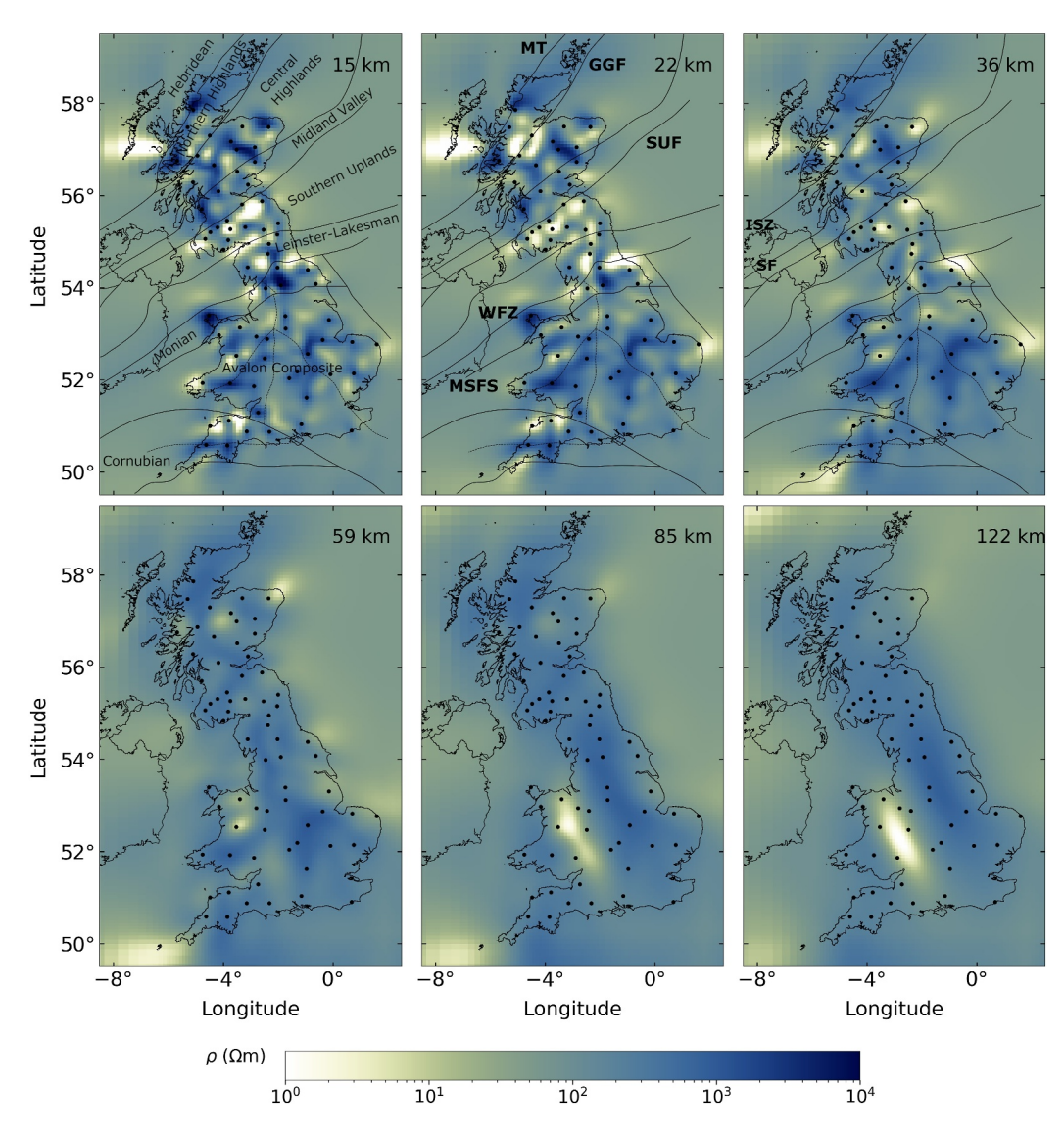


Figure 3. Horizontal slices of the final 3D resistivity model at different crustal and mantle depths.

changes higher than 5%. From these sites, all but two show a positive change, indicating increased misfits. All changes occur in the longest periods, with a 59% relative change for the decade 1,000–11,000 s. Of the sites that do not show a significant change, five do not have data in the sensitive decade, and three others have noisy data such that, although there are changes in the response, they are not reflected in the site RMS misfits as they still are within the error bars. Therefore, these results indicate that the data are sensitive to resistivity to depths of 200 km. Furthermore, they show that an increased resistivity of 200  $\Omega$ m is not acceptable at those depths, which is consistent with the expected lower resistivities at asthenospheric depths.

In a similar fashion, we tested the sensitivity of the data to the presence of the West Midlands conductor. In the region where the deep conductive anomaly appears (between 85 and 200 km depth), we modified the resistivity of all cells with values below 50  $\Omega$ m, increasing them to 200  $\Omega$ m, which is the average resistivity of surrounding cells at those depths. We then computed the forward response of this perturbed model and found that the RMS misfit increased at most of the sites in and around the conductor (Figure 5), reaching a misfit increase of up to 43% at site SN72. An exception was site SH54 (located northwest from the conductor), where the fit improved by 5.6%. To try to constrain the base of the conductor, we also removed the conductor layer by layer, from 200 km upwards. Sites near the anomaly, including those from Figure 5, show sensitivity to changes below  $\sim$ 140 km, suggesting that below this depth there could be a smearing effect. We subsequently performed two inversions

12 of 20

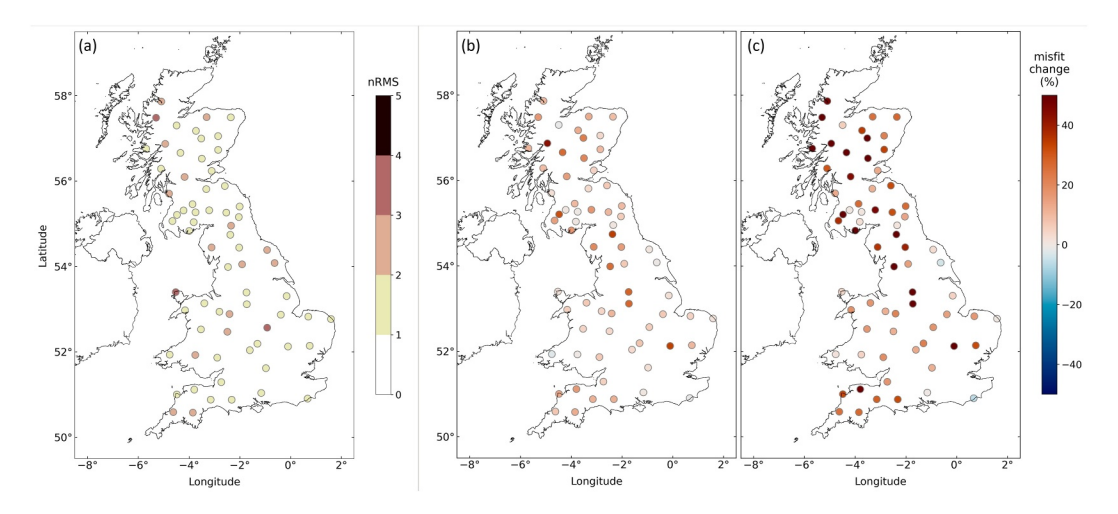
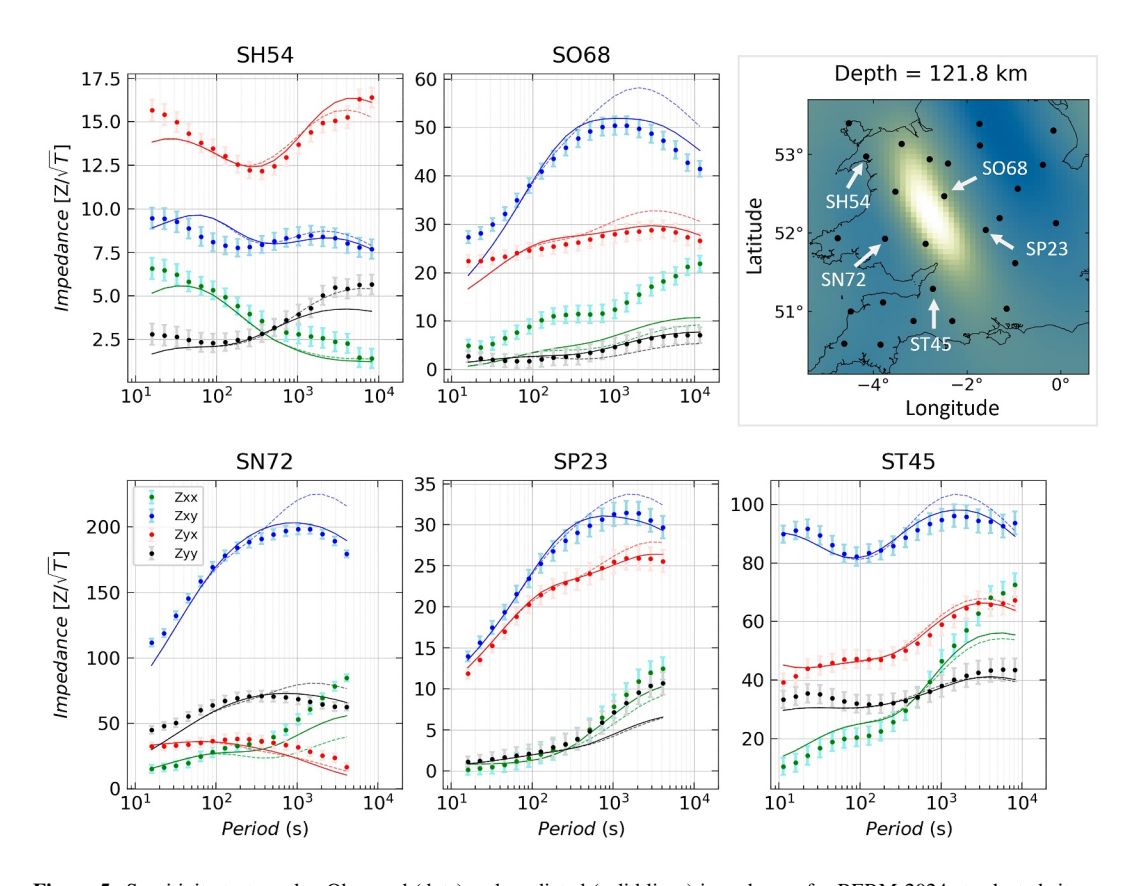


Figure 4. (a) RMS misfit at each site for the final model (BERM-2024). Relative misfit change (%) at each site after editing the resistivity of the final model below depths of (b) 280 km and (c) 200 km.

with the modified model. In the first inversion, we used it as starting model; in this case, the conductor was restored with slightly higher resistivity values. In the second inversion, we used the modified model as a prior model but forced the anomaly to be absent by fixing the modified cells. This resulted in higher misfits at more than half the sites in England and Wales compared to the misfits of BERM-2024.



**Figure 5.** Sensitivity test results: Observed (dots) and predicted (solid lines) impedances for BERM-2024 at selected sites above and around the deep conductor. The responses of the modified model, where the resistivity of the conductor was changed, are shown by dashed lines. Note that the data are plotted as the absolute value of the impedance components divided by the square root of the period to improve the visual comparison of the four components.

MONTIEL-ÁLVAREZ ET AL.

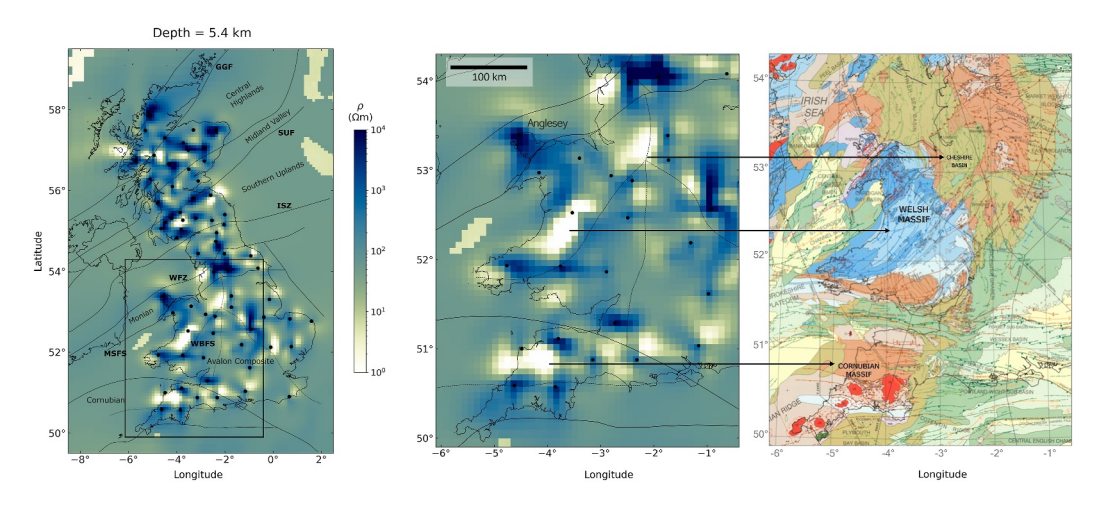


**Figure 6.** Final resistivity model at a depth of 5.4 km, showing relevant faults and terranes (left panel). Faults and terrane boundaries are labeled as in Figure 1. Model at the same depth with focus on western Britain (central panel) indicating the correlation between conductive anomalies and sedimentary basins on an extract of the Tectonic Map of Britain (British Geological Survey, 1996) (right panel).

By inspecting the models from initial inversion tests (in Section 3.3), we found that the resulting model from inverting only impedances also shows the conductor in the same location and orientation but with slightly higher resistivity than BERM-2024, while the model from inverting tippers shows a modest conductor with a similar orientation but with a reduced elongated extension and slightly displaced westwards. However, tippers do not show much sensitivity to the resistivity changes in these tests, which is likely due to the dominating effect of the ocean and marine sediments. The fact that there are no sites directly on top of the conductor may indicate that it is not fully resolved and more data would be ideal for further analysis. However, the different tests indicate that a strong conductor of similar orientation, lateral extension, and depth is needed by the data.

#### 4.2. Lithospheric Features in BERM-2024

In the presented model, we find strong spatial correlation between resistivity features (Figure 3) and geology. These will now be described.

At shallow crustal depths (~5 km), high-conductivity zones in western Britain coincide with sedimentary basins such as the Cheshire Basin, the Welsh Basin, and the Culm Basin in the Cornubian Massif (Figure 6). While the lateral resolution limits the precise delineation of their shape and boundaries, the correlation is strong. Although these basins are of different geologic age (Triassic, Silurian, and Carboniferous, respectively), their high conductivity can be explained by fluid saturation and similar lithology, which consists primarily of mudstones, siltstones, and sandstones. Clays and silt, the main component of mudstones and siltstones, exhibit high conductivity under wet conditions.

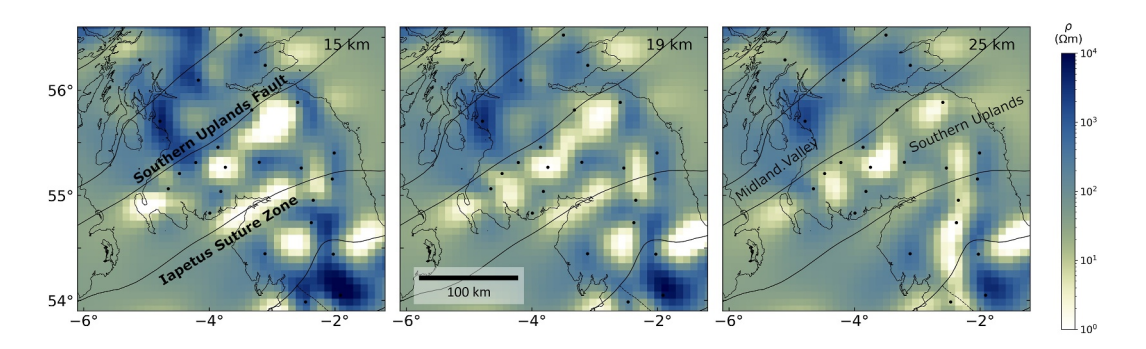


Figure 7. Final resistivity model at depths 15, 19 and 25 km with focus on the Southern Uplands and adjacent areas showing coastlines and main fault zones.

MONTIEL-ÁLVAREZ ET AL. 13 of 20

**Figure 8.** Final resistivity model at depths 22, 28 and 36 km with focus on northern Scotland around the Great Glen Fault (GGF) showing coastlines and main faults. Black arrows represent the relative movement along the GGF.

At the same depths, higher resistivity values found in the rest of the Welsh Basin as well as along the north boundary of the Southern Uplands terrane seem to correspond to Ordovician outcrops (see Molyneux et al., 2023). Other features of high resistivity coincide with known granitic plutons, that is, the EW anomaly in the Central Scottish Highlands appears to match the trend of plutons of the Cairngorm Suite, while in Cornwall, the anomaly south of the conductor in the Cornubian terrane coincides with the two largest plutons of the Cornubian batholith.

Inspecting the model at depths between 15 and 25 km depth, we find that the Southern Uplands Terrane in southern Scotland is underlain by a conductive anomaly (Figure 7). It extends along the terrane's northern margin, defining well the SUF and a clear contrast to a less conductive Midlands Valley terrane to the north. To the south, a thinner conductor along the ISZ may be linked to the Northumberland-Solway basin. Our results agree with previous studies that identified the presence of a conductor at mid-to low-crustal depths in the Southern Uplands and the Northumberland basin (e.g., Beamish, 1986; Parr & Hutton, 1993), and for the first time it is imaged here in three dimensions.

The conductor beneath the Southern Uplands Terrane extends to greater depths (up to 35 km) in the northeast and the central area. The latter confirms the presence of the lower crustal conductor beneath Eskdalemuir, as first identified by Edwards et al. (1971).

We further identify that in Anglesey, a small island off the north-west coast of Wales in the Monian Composite terrane, the model exhibits a distinct high resistivity anomaly from the surface down to the base of the crust at about 30 km (see top panels in Figure 3). Between 17 and 40 km depth, lateral variations to more conductive zones north and south of the Monian terrane align with the Wicklow Fault Zone and Menai Strait Fault System (MSFS) respectively.

Two conductive anomalies are observed on both sides of the Great Glen Fault (GGF) starting at around 18 km depth (Figure 8). These seem to be displaced relative to each other with an increase in offset at greater depths down to 40 km. This offset could be evidence of displacement along the fault, as it coincides with known early sinistral displacement.

Furthermore, we observe two additional conductive anomalies appearing between 20 and  $\sim$ 35 km depth. One forms an elongated structure aligned approximately north-south, crossing the Leinster-Lakesman Terrane and the Monian Composite, while the other is located along the Stainmore Fault (SF) and near the east coast (e.g., Figure 7). These anomalies do not directly correspond to known geological or tectonic structures.

Finally, we identify an intriguing conductor between  $\sim$ 85 and 140 km depth (Figure 9). This anomaly, now referred to as the "West Midlands conductor," has not been described in previous geophysical studies. As discussed in Section 4.1, additional data on top of the conductor would be ideal to further constrain and study the anomaly.

We conclude our model description with the observation that most strong resistivity variations occur within the crust. Some conductors remain well defined down to  $\sim$ 45 km, in the uppermost mantle. Below this depth, the resistivity distribution becomes largely homogeneous, with only the roots of some conductors still visible but less pronounced. However, a newly identified, prominent conductor stands out between  $\sim$ 85–140 km. Future work

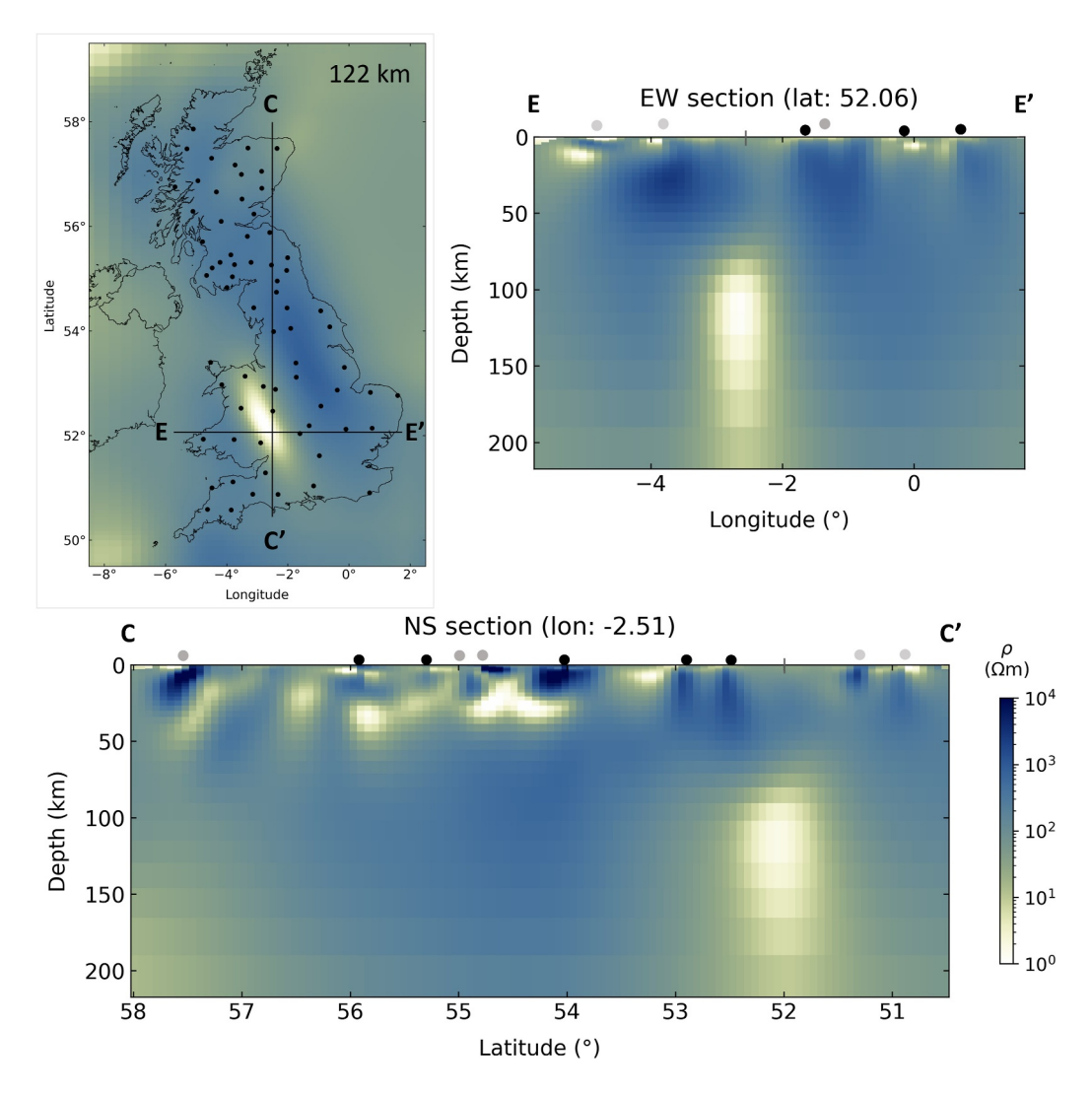


**Figure 9.** Cross-sections from the 3D resistivity model showing the West Midlands conductor. The vertical exaggeration is 1.65. Black dots above the cross-sections represent MT sites located directly along the profile, while gray dots indicate projected location of nearby sites that are not exactly on the profile.

will focus on integrated interpretation or multi-physics inversion to further investigate the new detected anomalies.

#### 5. Application to Space Weather Hazard Modeling

In addition to the significance for geological studies, the new 3D electrical resistivity model (or BERM-2024) has an important application in assessing the risk of solar activity or space weather in modern society. Rapid variations of the Earth's magnetic field during space weather events induce electric currents to flow in the Earth. These so-called geomagnetically induced currents (GICs) can enter and damage grounded infrastructure such as high voltage (HV) power networks, railways and pipelines. To model and forecast GICs, the geoelectric field at the Earth's surface needs to be known during the geomagnetic storm. Previous studies used thin-sheet modeling with lithological constraints to estimate the induced ground electric field during large geomagnetic storms in Britain and their effect on the HV power grid (e.g., Beggan, 2015; Kelly et al., 2017). Improving the ground electric field model for Britain was the primary objective of the LMT data collection campaign. The geoelectric field depends directly on the ground conductivity, and there are several approaches to estimate it. One method commonly applied uses the measured MT impedances and real-time geomagnetic field observations directly through Equation 1 (e.g., Cordell et al., 2021; Kelbert et al., 2017; Malone-Leigh et al., 2023). Hübert, Eaton,

MONTIEL-ÁLVAREZ ET AL. 15 of 20

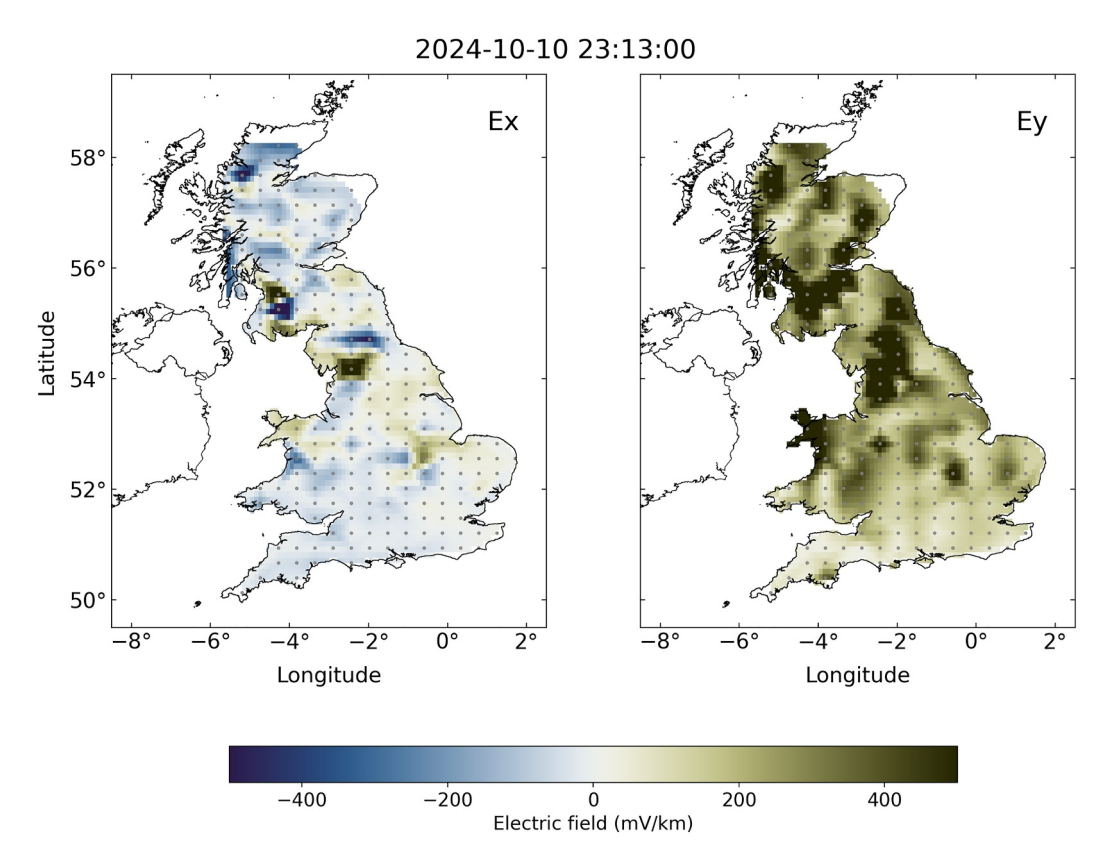


Figure 10. North-south  $(E_x)$  and east-west  $(E_y)$  component of the geoelectric field modeled for 10 October 2024 23:13:00 UTC using MT transfer functions extracted from BERM-2024 in a regular grid (gray dots).

Beggan, Montiel-Álvarez, et al. (2025) show this approach applied to our data set and explain the methodology in more detail. It is also possible to use impedance responses computed from an MT data-derived 3D conductivity model (e.g., Marshall et al., 2019; Zhang et al., 2024). This approach has the advantage that the conductivity distribution between sites is modeled during the inversion process and is physically more meaningful than the simple interpolation of impedances or geoelectric fields.

We investigate the capability of BERM-2024 to correctly model geoelectric fields for the whole of Britain during the severe G4 storm of 10–11 October 2024 implementing the simple approach of  $FFT^{-1}[Z(\omega) \cdot FFT(B_{SECS}(t))]$  (e.g., Campanyà et al., 2019; Malone-Leigh et al., 2023), derived from Equation 1, and adapting the code of Campanyà et al. (2019). Driving the variations in the ground electric field are the observations of the magnetic field. We used 2 days of 1-min magnetic field data measured at the three geomagnetic observatories (LER, ESK, HAD) and three variometer sites in the UK, and interpolated them over Britain using the Spherical Elementary Current System (SECS) approach (McLay & Beggan, 2010) ( $B_{SECS}$ ). From our 3D resistivity model, BERM-2024, we computed MT impedances at locations on a 30 km regular grid for the period range of 11–11,000 s with ModEM. The full FFT is applied to the interpolated magnetic fields to convolve them with the MT impedances ( $Z(\omega)$ ) in the complex domain. Finally, the  $FFT^{-1}$  is applied to predict the real-valued geoelectric field in the time domain. We obtained time-series of horizontal geoelectric field ( $E_x$  and  $E_y$ ) at each point of the 30 km regular grid with the same sampling rate as the magnetic fields (1 min).

The peak of the geomagnetic storm is defined as the minute when the sum of the absolute geoelectric field values across all sites in the regular grid reaches its maximum. Figure 10 shows a snapshot of the horizontal components of the geoelectric field during the peak time of the storm (Kp = 9-) on October 10 at 23:13 UTC. We obtained maximum field values of 1.9 V/km, with the highest amplitudes observed in Anglesey, Scotland, and northern England. The overall largest fields across Britain average ~400 mV/km. In general, the east-west ( $E_y$ ) component shows higher amplitudes than the north-south ( $E_x$ ) one.

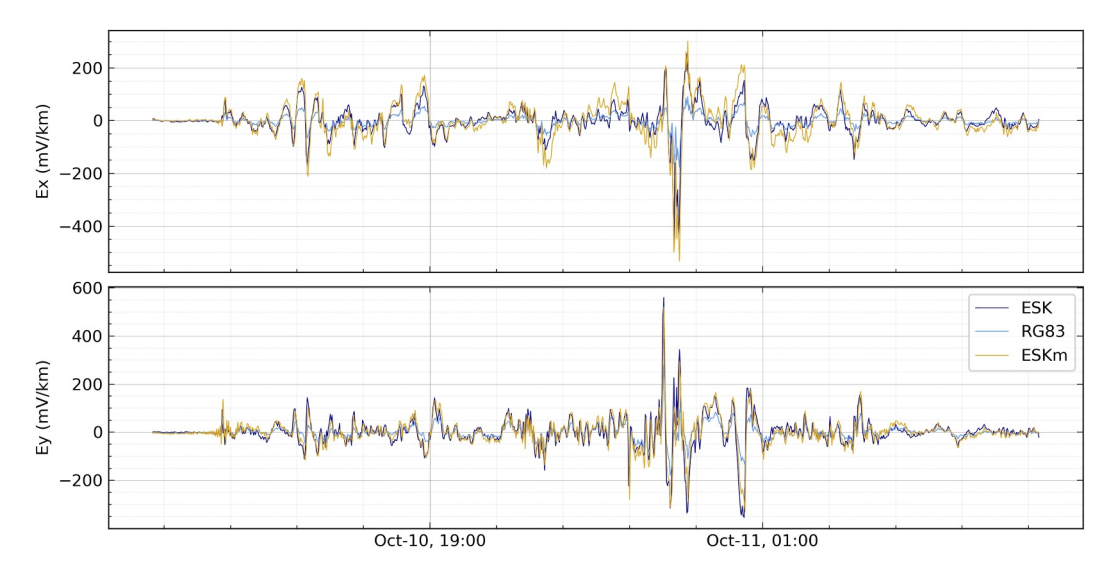


Figure 11. Comparison of geoelectric field components  $E_x$  and  $E_y$  measured at Eskdalemuir magnetic observatory (ESK, dark blue), modeled at the ESK location (ESKm, yellow), and modeled at the closest location of the regular grid (RG83, light blue).

For model verification, we compare the electric fields measured at Eskdalemuir observatory (ESK) with the modeled estimates from BERM-2024 (ESKm) and from the regular grid, at the closest location to ESK (RG83) (Figure 11). RG83 is about 12 km south-west of ESK, which is effectively only one cell apart in the model. Nonetheless, there are considerable resistivity differences between the two locations across crustal depths (down to 32 km). There is high correlation between the fields with correlation coefficients of 0.9 for  $E_x$  and 0.78 for  $E_y$  between ESK and ESKm. The amplitudes of the modeled fields at RG83 are considerably smaller than those measured at the ESK observatory. This may be due to the resistivity differences in the model, which are reflected as lower apparent resistivity at RG83 compared to ESK. However, we can see that the amplitudes are much better recovered when using the impedances from the exact location ESKm (although slightly overestimated for  $E_x$ ).

These results show that high correlation and accurate amplitude recovery can be achieved using impedances from a data-driven 3D resistivity model at MT site locations. However, a significant decrease in amplitude is observed even at short distances from the site locations. Although the amplitude discrepancies require further investigation, it is clear that denser data grids and potentially higher frequencies are needed to improve resolution, as suggested by Murphy et al. (2021). Despite the underestimation of amplitudes, the model is robust as it describes the geoelectric field everywhere, accounting for resistivity variations in three dimensions.

#### 6. Conclusions

This study presents the first three-dimensional (3D) lithospheric electrical resistivity model of Britain, derived from the inversion of long-period magnetotelluric data. The model provides new insights into the electrical conductivity distribution of the crust and upper mantle and establishes a foundation for future geophysical studies. It is also an important part in the assessment of space weather hazard on grounded infrastructure.

The methodology developed and applied in this study optimized the MT inversion workflow through systematic testing of prior models, inversion strategies, and regularization parameters to ensure a robust final model. The presented tests highlight the importance of incorporating detailed bathymetry and resistivity variation of marine sediments as they significantly impacted the inversion results. Despite these advancements, certain limitations remain. The lack of MT data at higher frequencies restricts the resolution of the model in the shallow crust, which could be one of the causes for the underestimation of geoelectric fields at locations without MT sites.

The resistivity model reveals significant lateral and vertical variations that correlate with known geological and tectonic features. At shallow crustal depths, several high-conductivity anomalies align with sedimentary basins in western Britain, while resistive anomalies show correspondence with granite plutons in Scotland and Cornwall

and with Ordovician outcrops across Britain. The Southern Uplands and the Northumberland-Solway Basin exhibit mid-crustal conductors that extend to depths of  $\sim 35$  km, in agreement with previous studies and defining the extent of the anomaly in three dimensions. Additionally, a prominent deep conductor is identified between 85 and 140 km depth beneath the West Midlands region, with no direct geophysical precedent. Future research will focus on multi-physics approaches to incorporate additional geophysical and petrological data, to refine the interpretation of the lithospheric structure beneath Britain.

Beyond geological implications, the resistivity model plays a role in space weather hazard assessments by providing new information for geoelectric field modeling. The application to the geomagnetic storm of 10–11 October 2024 indicates a high correlation between modeled and observed electric fields, though amplitude discrepancies remain to be accounted for. Investigating these differences will enhance the monitoring and prediction of geomagnetically induced currents (GICs) and their potential impact on power grids and other infrastructure.

Overall, this study establishes a baseline model for future local geophysical investigations in Britain, providing a valuable resource for understanding lithospheric structures and space weather interactions, and underscores the need for continued MT data acquisition and methodological improvements to further refine resistivity models and their applications to space weather.

#### **Data Availability Statement**

The SAGE and SWIGS LMT data are freely available at the National Geoscience Data Centre (NGDC) from Hübert, Eaton, Beggan, Collins, and Wang (2025), Montiel-Álvarez et al. (2025), Hübert and Beggan (2022a, 2022b), Simpson and Bahr (2020). Magnetic data from the UK observatories are available on INTERMAGNET. We used the Scientific colour maps from Crameri (2018) for maps and model plots.

#### References

Allen, M. (2019). The long and moving story of the Great Glen Fault. The Mercian Geologist, 19(4), 216-223.

Bailey, R. C., & Edwards, R. N. (1976). The effect of source field polarization on geomagnetic variation anomalies in the British Isles. *Geophysical Journal of the Royal Astronomical Society*, 45(1), 97–104. https://doi.org/10.1111/j.1365-246X.1976.tb00315.x

Banks, R. J., Livelybrooks, D., Jones, P., & Longstaff, R. (1996). Causes of high crustal conductivity beneath the Iapetus suture zone in Great Britain. *Geophysical Journal International*, 124(2), 433–455. https://doi.org/10.1111/j.1365-246X.1996.tb07031.x

Baykiev, E., Guerri, M., & Fullea, J. (2018). Integrating gravity and surface elevation with magnetic data: Mapping the curie temperature beneath the British Isles and surrounding areas. Frontiers in Earth Science, 6, 165. https://doi.org/10.3389/feart.2018.00165

Beamish, D. (1986). Deep crustal geoelectric structure beneath the Northumberland Basin. *Geophysical Journal International*, 84(3), 619–640. https://doi.org/10.1111/j.1365-246X.1986.tb04374.x

Beggan, C. D. (2015). Sensitivity of geomagnetically induced currents to varying auroral electrojet and conductivity models. *Earth Planets and Space*, 67(1), 24. https://doi.org/10.1186/s40623-014-0168-9

Bluck, B. J., Gibbons, W., & Ingham, J. K. (1992). Terranes. *Geological Society*, 13, 1–4. https://doi.org/10.1144/GSL.MEM.1992.013.01.03
Bott, J., Scheck-Wenderoth, M., Kumar, A., Cacace, M., Noe, S., & Faleide, J. I. (2024). Density and strength variations in the mantle lithosphere affect the distribution of intraplate earthquakes. *Communications Earth & Environment*, 5(1), 243. https://doi.org/10.1038/s43247-024-

British Geological Survey. (1996). Tectonic Map of Britain, Ireland and adjacent areas. Retrieved from https://webapps.bgs.ac.uk/data/maps/maps.cfc?method=viewRecord&mapId=12085

Campanyà, J., Gallagher, P. T., Blake, S. P., Gibbs, M., Jackson, D., Beggan, C. D., et al. (2019). Modeling geoelectric fields in Ireland and the UK for space weather applications. *Space Weather*, 17(2), 216–237. https://doi.org/10.1029/2018SW001999

Cocks, L., & Fortey, R. (1982). Faunal evidence for oceanic separations in the palaeozoic of Britain. *Journal of the Geological Society*, 139(4), 465–478. https://doi.org/10.1144/gsigs.139.4.0465

Cordell, D., Unsworth, M. J., Lee, B., Hanneson, C., Milling, D. K., & Mann, I. R. (2021). Estimating the geoelectric field and electric power transmission line voltage during a geomagnetic storm in Alberta, Canada using measured magnetotelluric impedance data: The influence of three-dimensional electrical structures in the lithosphere. *Space Weather*, 19(10), e2021SW002803. https://doi.org/10.1029/2021SW002803 Crameri, F. (2018). *Scientific colour maps*. Zenodo. https://doi.org/10.5281/zenodo.1243862

Crameri, F., Shephard, G. E., & Heron, P. J. (2020). The misuse of colour in science communication. *Nature Communications*, 11(1), 5444. https://doi.org/10.1038/s41467-020-19160-7

Davis, M. W., White, N. J., Priestley, K. F., Baptie, B. J., & Tilmann, F. J. (2012). Crustal structure of the British Isles and its epeirogenic consequences. *Geophysical Journal International*, 190(2), 705–725. https://doi.org/10.1111/j.1365-246X.2012.05485.x

Dewey, J. F. (1969). Evolution of the Appalachian/Caledonian orogen. *Nature*, 222(5189), 124–129. https://doi.org/10.1038/222124a0 Dong, S. W., Li, T. D., Lü, Q. T., Gao, R., Yang, J. S., Chen, X. H., et al. (2013). Progress in deep lithospheric exploration of the continental China: A review of the sinoprobe. *Tectonophysics*, 606, 1–13. https://doi.org/10.1016/j.tecto.2013.05.038

Edwards, R. N., Law, L. K., & White, A. (1971). Geomagnetic variations in the British Isles and their relation to electrical currents in the ocean and shallow seas. *Philosophical Transactions of the Royal Society of London*, 270(1204), 289–323. https://doi.org/10.1098/rsta.1971.0076

Egbert, G. D., & Kelbert, A. (2012). Computational recipes for electromagnetic inverse problems. *Geophysical Journal International*, 189(1), 251–267. https://doi.org/10.1111/j.1365-246X.2011.05347.x

Acknowledgments

This work was funded under the UK Natural Environment Research Council (NERC) Grant SWIMMR (N4) NE/ V002694/1 and the NERC Doctoral Training Partnership Grant NE/S007407/1. AM was additionally supported by CONAHCYT Abroad Scholarships and the BGS Universities Funding Initiative (BUFI Student S462). AM thanks the Scottish Alliance for Geoscience, Environment and Society (SAGES) and the Royal Astronomical Society (RAS) for the grants that enabled additional acquisition of LMT data in Scotland. This work used the Cirrus UK National Tier-2 HPC Service at EPCC (http://www.cirrus. ac.uk) funded by the University of Edinburgh and EPSRC (EP/P020267/1). We thank Anna Kelbert, Gary Egbert and Naser Meqbel for making ModEM and 3Dgrid available. We are grateful to Maxim Smirnov for providing the KMSproMT processing software and to Alexander Gravver for kindly sharing ocean and sediment conductance models for the UK. The results presented in this paper rely on data collected at magnetic observatories. We thank the national institutes that support them and INTERMAGNET for promoting high standards of magnetic observatory practice (www.intermagnet.org). The scientific color maps from Crameri (2018) were used in this study to prevent visual distortion of the data and exclusion of readers with color-vision deficiencies (Crameri et al., 2020). We encourage the EM induction community to adopt perceptually-uniform color maps. Finally, we thank the BGS staff who helped with the long-period MT data acquisition campaign, especially Eliot Eaton, Adam Collins, and Guanren Wang, as well as the landowners who very graciously granted

access to their land for the MT

installations

Wiley Online Library on [10/11/2025]. See the Term.

2025



## Journal of Geophysical Research: Solid Earth

- 10.1029/2025JB031813
- Gamble, T. D., Goubau, W. M., & Clarke, J. (1979). Magnetotellurics with a remote magnetic reference. *Geophysics*, 44(1), 53–68. https://doi.org/10.1190/1.1440923
- GEBCO Compilation Group. (2023). GEBCO 2023 Grid [Dataset]. https://www.gebco.net/data\_and\_products/gridded\_bathymetry\_data/doi:10. 5285/f98b053b-0cbc-6c23-e053-6c86abc0af7b
- Goubau, W. M., Gamble, T. D., & Clarke, J. (1978). Magnetotelluric data analysis: Removal of bias. Geophysics, 43(6), 1157–1166. https://doi. org/10.1190/1.1440885
- Grayver, A. V. (2021). Global 3-D electrical conductivity model of the world ocean and marine sediments. Geochemistry, Geophysics, Geosystems, 22(9), e2021GC009950. https://doi.org/10.1029/2021GC009950
- Grayver, A. V., Munch, F. D., Kuvshinov, A. V., Khan, A., Sabaka, T. J., & Tøffner-Clausen, L. (2017). Joint inversion of satellite-detected tidal and magnetospheric signals constrains electrical conductivity and water content of the upper mantle and transition zone. *Geophysical Research Letters*, 44(12), 6074–6081. https://doi.org/10.1002/2017GL073446
- Hanneson, C., & Unsworth, M. J. (2023). Magnetotelluric imaging of the magmatic and geothermal systems beneath Mount Meager, southwestern Canada. Canadian Journal of Earth Sciences, 60(10), 1385–1403. https://doi.org/10.1139/cjes-2022-0136
- Harinarayana, T., Hutton, V. R. S., & Jones, P. C. (1993). Lateral variations of conductivity structure across Southern Scotland and Northern England. Physics of the Earth and Planetary Interiors, 81(1–4), 25–41. https://doi.org/10.1016/0031-9201(93)90122-p
- Hautot, S., Single, R. T., Watson, J., Harrop, N., Jerram, D. A., Tarits, P., et al. (2007). 3-D magnetotelluric inversion and model validation with gravity data for the investigation of flood basalts and associated volcanic rifted margins. *Geophysical Journal International*, 170(3), 1418–1430. https://doi.org/10.1111/j.1365-246X.2007.03453.x
- Holdsworth, R. E., Woodcock, N. H., & Strachan, R. A. (2012). Geological framework of Britain and Ireland. In *Geological history of Britain and Ireland* (2nd ed., pp. 19–39). John Wiley and Sons. https://doi.org/10.1002/9781118274064.ch2
- Hübert, J., & Beggan, C. (2022a). Magnetotelluric time series for site Dalry (DAL) [Dataset]. NERC EDS National Geoscience Data Centre. https://doi.org/10.5285/c934280d-ca18-4aeb-9caf-084d08564b56
- Hübert, J., & Beggan, C. (2022b). Magnetotelluric time series for site Whiteadder (WHI) [Dataset]. NERC EDS National Geoscience Data Centre. https://doi.org/10.5285/23d18e2f-c612-4c46-bb43-f424869df25c
- Hübert, J., Beggan, C. D., Richardson, G. S., Gomez-Perez, N., Collins, A., & Thomson, A. W. (2024). Validating a UK geomagnetically induced current model using differential magnetometer measurements. *Space Weather*, 22(2), e2023SW003769. https://doi.org/10.1029/2023SW003769
- Hübert, J., Eaton, E., Beggan, C. D., Collins, A., & Wang, G. (2025). Long-period Magnetotelluric data collected at 44 sites in Scotland, England and Wales [Dataset]. NERC EDS National Geoscience Data Centre. https://doi.org/10.5285/14274b67-86a5-4d9d-b3f4-20c6d20228d7
- Hübert, J., Eaton, E., Beggan, C. D., Montiel-Álvarez, A. M., Kiyan, D., & Hogg, C. (2025). Developing a new ground electric field model for geomagnetically induced currents in Britain based on long-period magnetotelluric data. Space Weather. https://doi.org/10.1029/ 2025SW004427
- Huebert, J., Eaton, E., & Beggan, C. D. (2022). Developing a UK new ground electric field model for SWIMMR N4 (SAGE) Interim Report (Tech. Rep.). British Geological Survey. www.bgs.ac.uk/gsni/
- Ingham, M. R., & Hutton, V. R. (1982). Crustal and upper mantle electrical conductivity structure in Southern Scotland. Geophysical Journal of the Royal Astronomical Society, 69(3), 579–594. https://doi.org/10.1111/j.1365-246X.1982.tb02764.x
- Ivannikova, E., Kruglyakov, M., Kuvshinov, A., Rastätter, L., & Pulkkinen, A. (2018). Regional 3-D modeling of ground electromagnetic field due to realistic geomagnetic disturbances. Space Weather, 16(5), 476–500. https://doi.org/10.1002/2017SW001793
- Jegen, M., Avdeeva, A., Berndt, C., Franz, G., Heincke, B., Hölz, S., et al. (2016). 3-D magnetotelluric image of offshore magmatism at the Walvis Ridge and rift basin. *Tectonophysics*, 683, 98–108. https://doi.org/10.1016/j.tecto.2016.06.016
- Jones, A. G., & Hutton, R. (1979a). A multi-station magnetotelluric study in southern Scotland I. Fieldwork, data analysis and results. Geophysical Journal of the Royal Astronomical Society, 56(2), 329–349. https://doi.org/10.1111/j.1365-246X.1979.tb00168.x
- Jones, A. G., & Hutton, R. (1979b). A multi-station magnetotelluric study in southern Scotland—II. Monte-Carlo inversion of the data and its geophysical and tectonic implications. Geophysical Journal of the Royal Astronomical Society, 56(2), 351–368. https://doi.org/10.1111/j.1365-246X.1979.tb00169.x
- Kelbert, A., Balch, C. C., Pulkkinen, A., Egbert, G. D., Love, J. J., Rigler, E. J., & Fujii, I. (2017). Methodology for time-domain estimation of storm time geoelectric fields using the 3-D magnetotelluric response tensors. *Space Weather*, 15(7), 874–894. https://doi.org/10.1002/20173W001594
- Kelbert, A., Bedrosian, P. A., & Murphy, B. S. (2019). The first 3D conductivity model of the contiguous United States: Reflections on geologic structure and application to induction hazards. In *Geomagnetically induced currents from the sun to the power grid* (pp. 127–151). wiley. https://doi.org/10.1002/9781119434412.ch8
- Kelbert, A., Meqbel, N., Egbert, G. D., & Tandon, K. (2014). ModEM: A modular system for inversion of electromagnetic geophysical data. Computers & Geosciences, 66, 40–53. https://doi.org/10.1016/j.cageo.2014.01.010
- Kelly, G. S., Viljanen, A., Beggan, C. D., & Thomson, A. W. (2017). Understanding GIC in the UK and French high-voltage transmission systems during severe magnetic storms. Space Weather, 15(1), 99–114. https://doi.org/10.1002/2016SW001469
- Leggett, J. K., Mckerrow, W. S., & Eales, M. H. (1979). The Southern Uplands of Scotland: A lower Palaeozoic accretionary prism. *Journal of the Geological Society*, 136(6), 755–770. https://doi.org/10.1144/gsjgs.136.6.0755
- Licciardi, A., England, R. W., Piana Agostinetti, N., & Gallagher, K. (2020). Moho depth of the British Isles: A probabilistic perspective. Geophysical Journal International, 221(2), 1384–1401. https://doi.org/10.1093/gjij/ggaa021
- Lindsey, N. J., & Newman, G. A. (2015). Improved workflow for 3D inverse modeling of magnetotelluric data: Examples from five geothermal systems. Geothermics, 53, 527–532. https://doi.org/10.1016/j.geothermics.2014.09.004
- Livelybrooks, D., Banks, R. J., Parr, R. S., & Hutton, V. R. S. (1993). Inversion of electromagnetic induction data for the lapetus Suture Zone in the UK. *Physics of the Earth and Planetary Interiors*, 81(1–4), 67–84. https://doi.org/10.1016/0031-9201(93)90124-r
- Malone-Leigh, J., Campanyà, J., Gallagher, P. T., Neukirch, M., Hogg, C., & Hodgson, J. (2023). Nowcasting geoelectric fields in Ireland using magnetotelluric transfer functions. *Journal of Space Weather and Space Climate*, 13(46), 6. https://doi.org/10.1051/swsc/2023004
- Marshall, R. A., Wang, L., Paskos, G. A., Olivares-Pulido, G., Van Der Walt, T., Ong, C., et al. (2019). Modeling geomagnetically induced currents in Australian power networks using different conductivity models. *Space Weather*, 17(5), 727–756. https://doi.org/10.1029/2018SW002047
- McLay, S. A., & Beggan, C. D. (2010). Interpolation of externally-caused magnetic fields over large sparse arrays using spherical elementary current systems. *Annales Geophysicae*, 28(9), 1795–1805. https://doi.org/10.5194/angeo-28-1795-2010

MONTIEL-ÁLVAREZ ET AL. 19 of 20



## Journal of Geophysical Research: Solid Earth

- 10.1029/2025JB031813
- Meqbel, N. M., Egbert, G. D., Wannamaker, P. E., Kelbert, A., & Schultz, A. (2014). Deep electrical resistivity structure of the northwestern U.S. derived from 3-D inversion of USArray magnetotelluric data. Earth and Planetary Science Letters, 402(C), 290–304. https://doi.org/10.1016/j.epsl.2013.12.026
- Miensopust, M. P. (2017). Application of 3-D electromagnetic inversion in practice: Challenges, pitfalls and solution approaches. *Surveys in Geophysics*, 38(5), 869–933. https://doi.org/10.1007/s10712-017-9435-1
- Molyneux, S. G., Harper, D. A. T., Cooper, M. R., Philip Hollis, S., Raine, R. J., Rushton, A. W. A., et al. (2023). A synopsis of the Ordovician System in its birthplace Britain and Ireland. *Geological Society, London, Special Publications*, 532(1), 191–266. https://doi.org/10.1144/sp532-2022-235
- Montiel-Álvarez, A., Collins, A., Wang, G., Hübert, J., & Beggan, C. (2025). Long-period magnetotelluric time-series collected at 9 sites in Scotland [Dataset]. NERC EDS National Geoscience Data Centre. https://doi.org/10.5285/1d5f975c-4a12-4c9d-8808-315afb33fe10
- Montiel-Álvarez, A., Hübert, J., & Whaler, K. (2022). Towards a new 3D conductivity model of the British Isles: Revisiting MT data from Isle of Skye, Scotland. Presented at the 25th Electromagnetic Induction Workshop. (Poster). https://doi.org/10.13140/RG.2.2.25587.75043
- Moorkamp, M., Özaydın, S., Selway, K., & Jones, A. G. (2022). Probing the Southern African lithosphere with Magnetotellurics—Part I: Model construction. *Journal of Geophysical Research: Solid Earth*, 127(3), e2021JB023117. https://doi.org/10.1029/2021JB023117
- Murphy, B. S., Lucas, G. M., Love, J. J., Kelbert, A., Bedrosian, P. A., & Rigler, E. J. (2021). Magnetotelluric sampling and geoelectric hazard estimation: Are national-scale surveys sufficient? *Space Weather*, 19(7), e2020SW002693. https://doi.org/10.1029/2020sw002693
- Osemeikhian, J. E., & Everett, J. E. (1968). Anomalous magnetic variations in Southwestern Scotland. Geophysical Journal of the Royal Astronomical Society, 15(4), 361–366. https://doi.org/10.1111/j.1365-246X.1968.tb00192.x
- Parkinson, W. D. (1962). The influence of continents and oceans on geomagnetic variations. Geophysical Journal of the Royal Astronomical Society, 6(4), 441–449. https://doi.org/10.1111/j.1365-246X.1962.tb02992.x
- Parr, R. S. (1991). Development of magnetotelluric processing and modelling procedures: Application to Northern England (Unpublished declared dissertation). University of Ediphyrch
- doctoral dissertation). University of Edinburgh.

  Parr, R. S., & Hutton, V. R. S. (1993). Magnetotelluric studies in and adjacent to the Northumberland Basin, Northern England. *Physics of the*
- Earth and Planetary Interiors, 81(1-4), 43-66. https://doi.org/10.1016/0031-9201(93)90123-q
  Robertson, K., Thiel, S., & Meqbel, N. (2020). Quality over quantity: On workflow and model space exploration of 3D inversion of MT data.
- Earth Planets and Space, 72(1), 2. https://doi.org/10.1186/s40623-019-1125-4
  Schultz, A. (2009). EMscope: A continental scale magnetotelluric observatory and data discovery resource. Data Science Journal, 8, IGY6–
- IGY20. https://doi.org/10.2481/dsj.ss\_igy-009
  Selway, K. (2014). On the causes of electrical conductivity anomalies in tectonically stable lithosphere. Surveys in Geophysics, 35(1), 219–257.
- https://doi.org/10.1007/s10712-013-9235-1
  Simpson, F., & Bahr, K. (2020). Magnetotelluric data from before, during and after the September 2017 magnetic storm at 7 sites in Scotland
- [Dataset]. British Geological Survey. https://doi.org/10.5285/59d3c54d-8179-4904-8ee7-1a81564ed893
- Smirnov, M. Y. (2003). Magnetotelluric data processing with a robust statistical procedure having a high breakdown point. *Geophysical Journal International*, 152, 1–7. https://doi.org/10.1046/j.1365-246x.2003.01733.x
- Stolz, N. (2013). New National Magnetotelluric (MT) survey gets underway. Retrieved from https://www.ga.gov.au/ausgeonews/ausgeonews201312/auslamp.jsp
- Tauber, S., Banks, R., Ritter, O., & Weckmann, U. (2003). A high-resolution magnetotelluric survey of the Iapetus suture zone in southwest Scotland. Geophysical Journal International, 153(3), 548–568. https://doi.org/10.1046/j.1365-246X.2003.01912.x
- Tietze, K., & Ritter, O. (2013). Three-dimensional magnetotelluric inversion in practice-the electrical conductivity structure of the San Andreas fault in central California. *Geophysical Journal International*, 195(1), 130–147. https://doi.org/10.1093/gji/ggt234
- Wilson, J. T. (1966). Did the Atlantic close and then re-open? Nature, 211(5050), 676-681. https://doi.org/10.1038/211676a0
- Zhang, X., Kong, W., Yu, N., Chen, H., Li, T., & Wang, E. (2024). Comparison of different geoelectric field methods to calculate geomagnetically induced currents in North China. *International Journal of Electrical Power & Energy Systems*, 155, 109657. https://doi.org/10.1016/j.ijepes. 2023.109657

MONTIEL-ÁLVAREZ ET AL. 20 of 20